

Collective Noise Filtering in Complex Networks

Tingyu Zhao^{1, 2} and István A. Kovács^{3, 4, 5, 2, *}

¹*Department of Industrial Engineering and Management Sciences,
Northwestern University, Evanston, Illinois 60208, USA*

²*NSF-Simons National Institute for Theory and Mathematics in Biology, Chicago, Illinois 60611, USA*

³*Department of Physics and Astronomy, Northwestern University, Evanston, Illinois 60208, USA*

⁴*Department of Engineering Sciences and Applied Mathematics,
Northwestern University, Evanston, Illinois 60208, USA*

⁵*Northwestern Institute on Complex Systems, Northwestern University, Evanston, Illinois 60208, USA*

(Dated: January 30, 2026)

Complex networks are powerful representations of complex systems across scales and domains, and the field is experiencing unprecedented growth in data availability. However, real-world network data often suffer from noise, biases, and missing data in the edge weights, which undermine the reliability of downstream network analyses. Standard noise filtering approaches, whether treating individual edges one-by-one or assuming a uniform global noise level, are suboptimal, because in reality both signal and noise can be heterogeneous and correlated across multiple edges. As a solution, we introduce the Network Wiener Filter, a principled method for collective edge-level noise filtering that leverages both network topology and noise characteristics, to reduce error in the observed edge weights and to infer missing edge weights. We demonstrate the broad practical efficacy of the Network Wiener Filter in two distinct settings, the genetic interaction network of the yeast *S. cerevisiae* and the Enron Corpus email network, noting compelling evidence of successful noise suppression in both applications. With the Network Wiener Filter, we advocate for a shift toward error-aware network science, one that embraces data imperfection as an inherent feature and learns to navigate it effectively.

Ever since the early development of graph theory, mathematicians have expanded its toolkit far beyond elegant puzzles, building increasingly sophisticated theories for reasoning about connectivity and structure [1]. In recent decades, network science transformed these abstract ideas into the empirical world, using networks to represent complex systems across diverse disciplines, including, among others, social science [2], biology [3], transportation [4], climate science [5], finance and economics [6]. Analyzing these complex systems from a network perspective has enabled researchers to uncover hidden patterns, capture emergent properties, and generate unique insights [7]. While the network science community has benefited from a rapid expansion in the availability of network data, it is frequently overlooked that such data can be imperfect. Real-world networks are often subjected to various kinds of errors such as noise, biases, and incomplete observation [8–11]. Yet it remains common in the literature to omit any quantitative assessment or reporting of these errors [12]. Moreover, most network analysis pipelines do not consider potential data errors and treat empirical networks as if they were exact graphs, in the spirit of graph theory. Ignoring the issue of data reliability in this manner can compromise the robustness of downstream network-based inference, leading to flawed conclusions and decisions.

In response, a growing body of work has sought to mitigate edge noise in network data by exploiting network topological information, including link prediction meth-

ods [13–21], diffusion-based methods [22–24], generative model-based methods [25–30], and singular value shrinkage methods [31–38]. Each method category relies on different, often strong, network structural assumptions and is tailored to different use cases (SI Table [placeholder]). However, none of these approaches is adequate for the realistic scenario of having heterogeneous and correlated noise. Either noise level is not explicitly incorporated, as in link prediction and diffusion-based methods, or noise is assumed to be largely homogeneous and independent across edges, as in generative model-based and singular value shrinkage methods. In the case of heterogeneous, or even correlated, noise, practitioners often resort to local thresholding strategies at the level of individual edges, without harnessing the rich information in the network architecture [11]. This, in turn, can limit the amount of signal that can be uncovered from the noisy data.

In this work, we propose the Network Wiener Filter (NetWF) as a principled method for collective noise filtering in complex networks. Grounded in the classical theory of Wiener filtering, the NetWF takes into account network topology through an intuitive edge-similarity measure, which is then combined with explicit edge-level noise statistics in a synergistic way. Importantly, this formulation naturally accommodates heterogeneous or correlated noise across edges, as well as the special case of homogeneous and independent noise, rendering it fully general with respect to noise structure. At the same time, the NetWF applies seamlessly to directed or undirected, binary, weighted or even signed networks. As illustrated on our real-world applications, our efficient implementation using the conjugate gradient algorithm enables the

* istvan.kovacs@northwestern.edu

NetWF to scale to large empirical networks.

FROM GENERALIZED WIENER FILTER TO THE NETWF

In classical signal processing, the Wiener filter is a foundational framework designed to recover the underlying true signal from noisy observations by minimizing the expected mean square error (MSE) between the estimate and the (unknown) true signal [39]. Using the statistical properties of both the signal and the noise, it seeks an optimal balance between noise suppression and signal preservation. As a result, Wiener filtering has been widely adopted for denoising tasks such as in time series (Figure 1A) and image processing (Figure 1B).

Generalized Wiener filter

Here, we start with a generalized Wiener filter formalism [40] and extend it to network data. Imagine that we observe a demeaned data vector $a = u + n \in \mathbb{R}^k$, where u denotes the true signal and n the additive noise. For data types that are not inherently one-dimensional, a can be understood as a vectorized representation, such as a vectorized image or a vectorized network adjacency matrix, $a = \text{vec}(A)$, where A_{ij} stands for the interaction weight between nodes i and j in the network. The goal is then to identify a “Wiener operator” G^W that, when acting on a , gives an estimate of the signal $\hat{u} = G^W a$ that minimizes the mean square error (MSE):

$$G^W = \arg \min_G \mathbb{E} \|G a - u\|_2^2, \quad (1)$$

where the expectation \mathbb{E} is taken over the joint realizations of u and n , and $\|\cdot\|_2$ is the L^2 norm. The optimization problem of Eq. 1 admits a closed-form analytical solution, see SI Text [placeholder]. In the case when u and n are drawn from independent distributions, the solution is given by

$$G^W = C_u (C_u + C_n)^{-1}, \quad (2)$$

in terms of the covariance matrices $C_u = \mathbb{E}[uu^T]$ and $C_n = \mathbb{E}[nn^T]$, both with dimensionality $\mathbb{R}^{k \times k}$.

Applying the Wiener filter hinges on having access to the two covariance matrices, or, more realistically, reliable proxies for them. C_n reflects noise characteristics and typically must be supplied through prior knowledge of how noise enters the data. In the simplest case, noise is independent and homogeneous, and C_n reduces to a scaled identity matrix, as we imposed in our illustrative examples in Figure 1. More generally, noise can be heterogeneous across entries, or even correlated, in which case C_n is a generic, positive semidefinite covariance matrix. On the other hand, C_u boils down to signal variability and correlation, where the latter can be interpreted

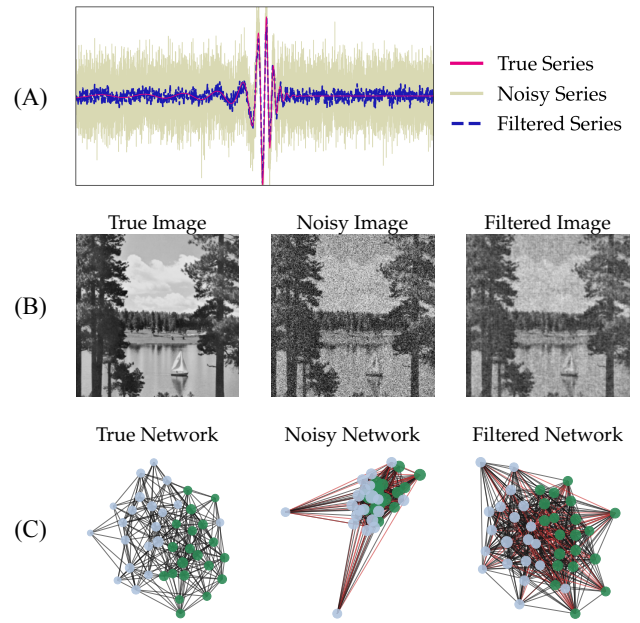


FIG. 1. **Illustration of Wiener filtering for noise reduction across data types, and why networks are different.** Starting from (A) a time series, (B) an image, and (C) a bipartite toy network, we add independent and identically distributed Gaussian white noise to obtain noisy observations. We then apply Wiener filtering to estimate the underlying signal from noisy observations using the known noise statistics (more details in SI Text [placeholder] and SI Figure [placeholder]). In time series and images, the classical Wiener filter exploits data-independent temporal or spatial proximity to capture signal correlations, with the intuition that nearby samples tend to be similar. In contrast, network data is inherently high-dimensional and requires a data-dependent adaptive treatment. The NetWF bridges this gap by using a network-informed edge-similarity measure that captures correlations globally across edges, as discussed in the main text. In the toy network, our NetWF reveals the original structure of two communities.

as the intrinsic similarity structure of the signal. For one-dimensional time series and two-dimensional images, this similarity structure is guided by proximity, as nearby samples are more similar than distant ones. Note that all images share the same grid-like proximity structure, independent of the actual pixel values. Then it is straightforward to specify a similarity structure that respects this regular grid architecture of the data, often *a priori* by positing a stationary kernel. It is also convenient to work in the frequency domain via the Fourier transform, where C_u can be described compactly by a power spectral density through the Wiener–Khintchin theorem, achieving high computational efficiency for the Wiener filter [39].

In contrast, networks (Figure 1C) are fundamentally different: the data is inherently high-dimensional with intricate correlations that depend on the input data. To

provide the required context for Wiener filtering, we must construct an edge-similarity measure that serves as the proxy for signal correlation in a qualitatively different, data-adaptive way, one that exploits the observed network patterns. In the proposed implementation of the NetWF, we do so using the intuition that edges between similar pairs of nodes are expected to be similar, as discussed next. As a result, in the example of Figure 1C the NetWF successfully reveals the original structure of two network communities.

Network-informed edge-similarity measure

For the purpose of community detection, a local notion of edge-similarity has been already proposed for edges that share an endpoint [41]. The fundamental idea is that any notion of node similarity can be used between the non-shared endpoints of the two edges to quantify the similarity of the edge pair. Here, we go one step beyond this local notion of edge-similarity and introduce a global edge-similarity between any two edges in the network, starting with the case of directed networks (Figure 2A). For two directed edges \overrightarrow{AB} and \overrightarrow{CD} , we separately model the similarity between the two source nodes, A and C , and between the two target nodes, B and D . As a convenient choice that works for any (binary, weighted or signed) networks, we quantify these node similarities using the Pearson correlation between their connection profiles. Specifically, the source profile similarity compares outgoing connection patterns,

$$s_{i,j}^{\text{source}} \equiv \text{corr}\left(w_{i \cdot}, w_{j \cdot}\right), \quad (3)$$

where $w_{i \cdot}$ collects the weights of edges pointing from node i to all other nodes. Likewise, the target profile similarity compares incoming connection patterns,

$$s_{i,j}^{\text{target}} \equiv \text{corr}\left(w_{\cdot i}, w_{\cdot j}\right), \quad (4)$$

where $w_{\cdot i}$ collects the weights of edges pointing from all other nodes to node i . Note that our NetWF framework is compatible with alternative notions of node similarity if desired, as also discussed later. As a last step, we then combine endpoint similarities to define the similarity between the directed edges \overrightarrow{AB} and \overrightarrow{CD} as

$$S_{\overrightarrow{AB}, \overrightarrow{CD}} \equiv s_{A,C}^{\text{source}} s_{B,D}^{\text{target}}. \quad (5)$$

For undirected networks (Figure 2B), nodes no longer play distinct source or target roles, and the profile similarity network (PSN) between two nodes is defined simply as

$$s_{i,j} \equiv \text{corr}\left(w_{i \cdot}, w_{j \cdot}\right), \quad (6)$$

where $w_{i \cdot}$ collects the weights of edges attached to node i . We obtain the similarity between the edge pair \overrightarrow{AB} and

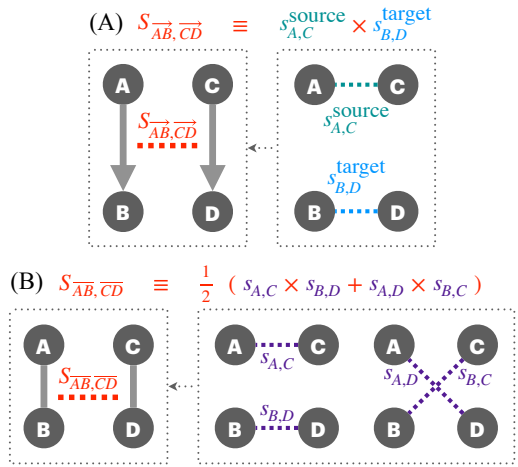


FIG. 2. **Construction of our global edge-similarity measure, a key ingredient in the NetWF.** We propose that edges are similar if their endpoints are similar. The similarity between two nodes is in turn quantified by correlating their connection profiles with all other nodes in the network. (A) In a directed network, for edges \overrightarrow{AB} and \overrightarrow{CD} , we separately consider the two sources (A vs. C) using their outgoing connection patterns and the two targets (B vs. D) using their incoming connection patterns (Eq. 5). (B) In an undirected network, the similarity between edges \overrightarrow{AB} and \overrightarrow{CD} is computed via considering the two configurations of endpoint matchings, yielding a label-invariant similarity measure (Eq. 7).

\overrightarrow{CD} by averaging over both configurations of endpoint matchings,

$$S_{\overrightarrow{AB}, \overrightarrow{CD}} \equiv \frac{1}{2}(s_{A,C} s_{B,D} + s_{A,D} s_{B,C}). \quad (7)$$

Although the Wiener filter appears to be a linear framework with respect to input data, the filtering process is actually nonlinear if the Wiener operator G^W of Eq. 2 itself is data-dependent, as is the case for the proposed NetWF. For detailed computational implementation of the NetWF, including a conjugate gradient-based iterative implementation that makes handling large empirical networks feasible, see the Materials and Methods.

APPLICATIONS IN REAL-WORLD COMPLEX NETWORKS

Next, we apply the NetWF to two real-world complex networks to assess its practical performance in two distinct settings: biological vs. social system, experimental vs. sampling noise, static vs. dynamic network, and undirected vs. directed edges. For comparison, we select the Optimal Shrinker (OS) of singular values as a state-of-the-art baseline noise filtering method [36]. The OS performs spectral compression by assuming that the adjacency matrix has low effective rank [38]. Although it applies broadly across network types, it is formulated

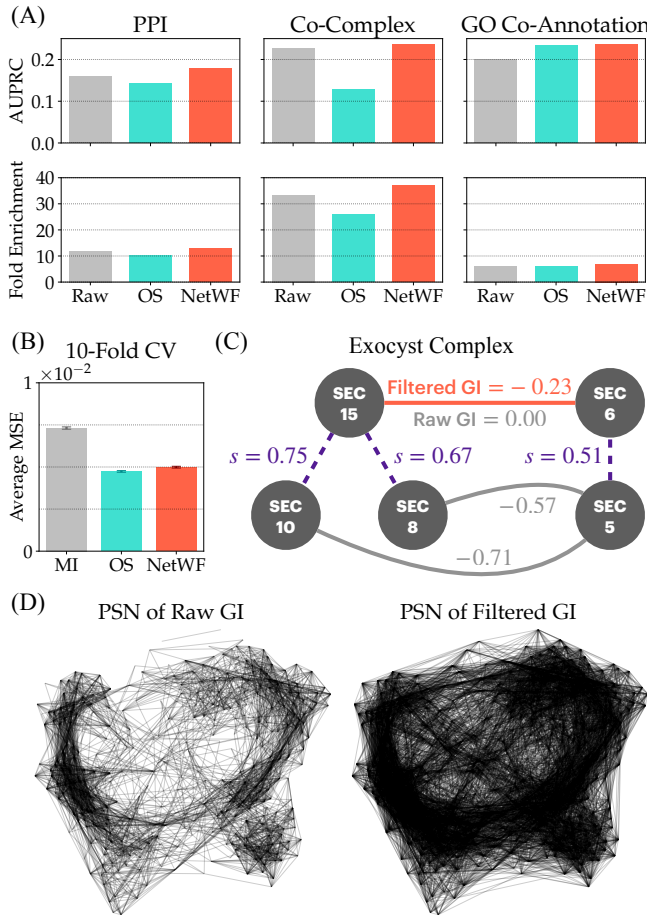


FIG. 3. Evidence that the NetWF reduces experimental noise in the yeast *S. cerevisiae* genetic interaction (GI) network. (A) Validation of negative GI values against three biological benchmarks: protein–protein interaction (PPI), protein co-complex membership, and Gene Ontology (GO) co-annotation. Relative to the raw data and the optimal shrinker (OS) baseline, NetWF improves both area under the precision–recall curve (AUPRC) and fold enrichment across all benchmarks. (B) A 10-fold cross validation (CV) test: in each fold, a random subset of GI entries is masked and predicted from the remaining data. The NetWF and the OS achieve significantly lower average mean square error (MSE) than naïve mean imputation (MI), where the missing entries are imputed using the mean of available GI values in each gene. Error bars indicate standard errors across folds. (C) Example of inferring a novel GI within the exocyst complex (SEC15–SEC6) by the NetWF. Dashed edges highlight a few example profile similarities within the complex that facilitate information propagation, collectively shifting the GI value from zero to a strongly negative estimate. (D) Profile similarity networks (PSNs) showcasing similarities between gene pairs (Eq. 6), before and after the NetWF is applied to the raw GI network. Edge width scales with similarity, and similarities below 0.2 are omitted for clarity.

for homogeneous noise only, so we need to homogenize heterogeneous noise in the input before applying the OS. See Materials and Methods for more details.

Biological network application: yeast genetic interaction network

Large-scale biological data are inherently noisy and incomplete, yet we rarely have detailed, quantitative insights into how much error there is in the measurements. A rare exception is the genome-wide pairwise genetic interaction (GI) network of the baker’s yeast *S. cerevisiae* [11]. Pairwise GIs arise when the fitness phenotype of a double mutant $f_{i,j}$ deviates from the expectation corresponding to independent single mutants fitness values, f_i and f_j :

$$\epsilon_{i,j} = f_{i,j} - f_i f_j. \quad (8)$$

Here, the fitness is measured as colony growth relative to a wild-type (non-mutant) reference under standardized conditions, via high-throughput synthetic genetic array (SGA) analysis [42]. Notably, as a result of the experiments, not only the $\epsilon_{i,j}$ edge weights are provided for each gene pair, but also the experimental error bar for each weight [11]. Most of the interaction weights were found to be comparable to the noise level, indicating that the independent baseline fitness expectation is valid for most gene pairs. A negative GI ($\epsilon_{i,j} < 0$) indicates that the double mutant grows worse than expected, in extreme cases known as synthetic lethality. Conversely, a positive GI ($\epsilon_{i,j} > 0$) indicates that the double mutant grows better than expected, i.e. genetic buffering or suppression. To identify true GIs, the authors suggested three alternative filtering approaches (lenient, intermediate, stringent) to the edge level data based on a combination of effects size ($\epsilon_{i,j}$) and noise reporting (p -value).

These systematic fitness screens uncovered a rich hierarchical functional organization in the eukaryotic cell, covering most of the pairwise GI space between $\sim 6,000$ genes in *S. cerevisiae*. The organization of GIs was found to be qualitatively different for essential genes (required for growth) vs. non-essential genes, as well as for positive vs. negative GIs. Here, as an illustration of the NetWF, we restrict our analysis to the dense part of the network between essential genes (ExE), comprising only temperature-sensitive alleles (427 nodes), see Materials and Methods for details. Besides providing rich functional information, it was also found that GIs are enriched in additional biological information. In the ExE space, this is manifested in the significant overlap between negative GIs and other data sources, including protein–protein interactions (PPI) [43], protein co-complex membership [42, 44], and Gene Ontology (GO) co-annotation [45], see Materials and Methods for details. The relatively few cases of extreme positive GIs also provide information on genetic function; however, positive GIs were deemed to be somewhat problematic, potentially being diluted with false positives, prompting focused experimental efforts on genetic suppression [46, 47].

Using a stringent weight threshold, $\epsilon < -0.12$ (negative) and $\epsilon > 0.16$ (positive), the filtered ExE map contains 274 positive GIs and 6,705 negative GIs. The

noise variance information entails heterogeneous but uncorrelated edge-level noise, corresponding to a diagonal noise covariance matrix C_n . After the NetWF denoising (SI Figure [placeholder]), using the stringent weight thresholds yields only 21 positive GIs (96% reduction in count) and 4,838 negative GIs (28% reduction in count), including 716 new negative GIs compared to the local filtering. Notably, the NetWF reduces disproportionately the number of (potentially problematic) positive GIs, while even unveiling previously neglected negative GIs. More importantly, the filtered ExE network demonstrates stronger adherence to all three benchmarks (PPI, co-complex, GO), improving both area under the precision-recall curve (AUPRC) and fold enrichment relative to the raw data (Figure 3A). Here, fold enrichment compares the representation of benchmark pairs among the 1,000 most negative GIs to their background frequency across all ExE pairs.

Next, as an illustration of link prediction performance, we carry out a 10-fold cross validation test (Figure 3B). We divide the observed symmetric GI entries into 10 partitions, and in each fold, we mask the partitioned entries to missing values and predict them from the remaining observations, see Materials and Methods for details. The NetWF delivers substantially lower MSE than a naïve mean imputation that fills missing entries using the mean of available GI values for each gene.

As a case study, we successfully recover a missing interaction from the input data within the exocyst complex [48]. The NetWF infers a strong negative GI between genes SEC15-SEC6 ($\epsilon = -0.23$), in agreement with the known biophysical interaction [49, 50]. Although the prediction originates from the NetWF processing collective information from the entire network, we provide an interpretation within the exocyst subgraph (Figure 3C). Notably, SEC15 is highly similar to SEC10 and SEC8 in GI profile, while SEC6 is similar to SEC5; therefore the strong negative GI of SEC10-SEC5 and SEC8-SEC5 contributes to the negative SEC15-SEC6 estimate. See SI Figure [placeholder] for the physical structure of the exocyst complex.

Finally, to quantify gene-level similarity, we construct profile similarity networks (PSNs) in which edge weights are Pearson correlations between GI profiles (Eq. 6). Using the originally proposed cutoff > 0.2 [11], the PSN has 3,686 edges before filtering and 11,108 edges after filtering (Figure 3D). This three-fold increase indicates fewer idiosyncratic differences in gene connection profiles, i.e. a smaller effective degrees of freedom. Together with the evidence that biological signal is preserved or even enhanced (Figure 3A), this supports a higher signal-to-noise ratio after filtering.

In comparison, the OS baseline behaves inconsistently across evaluations. It adheres worse to the PPI and protein co-complex benchmarks than even the raw data (Figure 3A), yet performs well in cross validation (Figure 3B), yields a dense PSN (18,247 edges), and also recovers the SEC15-SEC6 interaction ($\epsilon = -0.17$).

To test how much the performance of the NetWF depends on having access to the rich heterogeneous noise information, we run a restricted, homogenized-noise version in which we replace the heterogeneous variances by their mean, just like for the OS. The restricted results across the board change only marginally compared to those with the full NetWF, with over a 99% overlap in terms of negative GIs (SI Figure [placeholder]). This indicates that the NetWF can be a useful tool across various applications, even without detailed noise characterization, as also illustrated in our next application.

Social network application: the Enron Corpus email network

The Enron Corpus is a publicly available database containing internal email exchanges among key Enron employees in the years leading up to the company's famous bankruptcy in December 2001, and it has become a widely used resource for studying organizational communication patterns [51]. We use this dataset for two complementary goals. First, we demonstrate the performance of the NetWF in the case of heterogeneous and correlated noise covariance C_n , the highest level of noise characteristics. Second, we take the opportunity to embrace the more common empirical setting where no noise statistics is provided, and stress test the extent to which the NetWF can perform denoising under this far from optimal condition.

We focus on the year 2001, which spans the peak of the crisis. After removing self-emails, the dataset contains 12,684 time-stamped emails among 163 employees. We construct the full-year network as a weighted, directed email exchange frequency network, where each directed edge weight is the email frequency from sender to recipient (Figure 4A). The resulting network exhibits a clear core-periphery organization, suggesting complex social structure [52]. The full-year network is a temporal aggregate of a dynamic communication process. To examine temporal variability, we also construct the twelve calendar-month snapshots of 2001 (SI Figure [placeholder]), each of which can be viewed as a noisy sample of the underlying full-year network, where the finite observation window causes sampling fluctuations in the edge weights. An interesting denoising task is therefore to filter each calendar-month snapshot to bring it closer to the full-year network, which we use as a reference signal.

To address the first goal, we use month-to-month fluctuations to estimate edge-level noise covariance and use this information in the NetWF, producing twelve denoised calendar-month snapshots (SI Figure [placeholder]). For the OS baseline, only the mean variance over nodes extracted from the full noise covariance is used (SI Figure [placeholder]). October 2001 provides an illustrative example because of its historical significance: Enron's accounting fraud came to light, sharply accelerating the company's downfall. Relative to the full-year

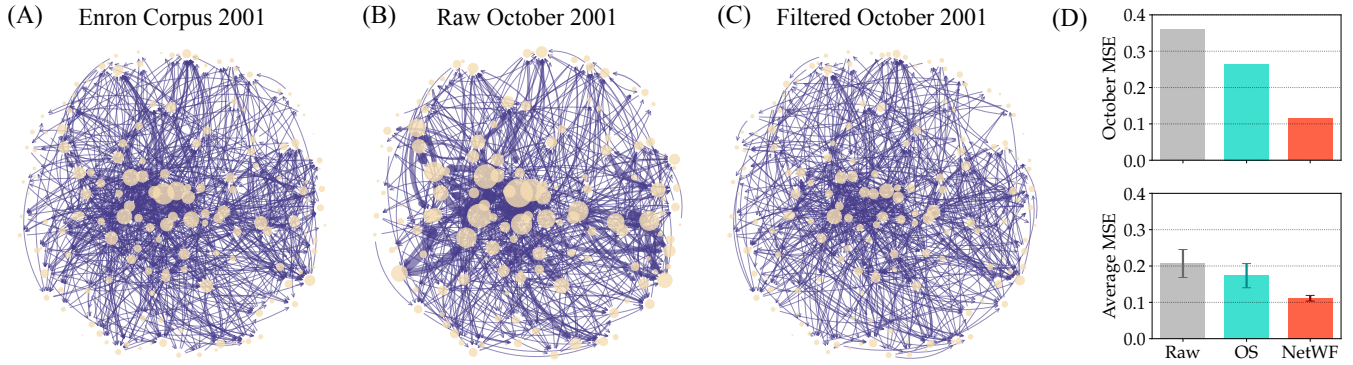


FIG. 4. **Evidence that the NetWF reduces sampling noise in the Enron Corpus email network.** (A) Full-year email exchange frequency network of 2001 between employees as nodes. Directed edges point from sender to recipient, with edge weight equal to email frequency (defined as the number of emails per month). Node size reflects the sum of incoming and outgoing weights. For clarity, edges with weight < 0.2 are not shown. (B) Raw October 2001 snapshot, treated as a noisy calendar-month sample of the full-year network, exhibiting pronounced fluctuations in edge weights. (C) October 2001 after applying the NetWF, with the extreme weights reduced without compromising the global structure. (D) Relative to the raw October network and the OS baseline, the NetWF largely reduces the October MSE with respect to the full-year network. Repeating for all twelve calendar-month snapshots, the NetWF also attains the lowest and most stable average MSE. Error bars indicate standard errors across calendar months.

network, the raw October snapshot shows turmoil with pronounced sampling fluctuations, including the presence of unusually strong edges (Figure 4B). After applying the NetWF, these extremes are smoothed while the global structure remains preserved (Figure 4C). Globally, in terms of the MSE with respect to the full-year network, the NetWF again outperforms both the raw snapshot and the OS. Over all twelve months, the NetWF achieves an average MSE of 0.11 ± 0.01 , lower and more robust compared to the raw snapshots (0.21 ± 0.04) and the OS outcomes (0.17 ± 0.03), as seen in Figure 4D. Similar evaluations carried out for each individual calendar-month snapshot, including both MSE and R^2 perspectives, are shown in SI Figure [placeholder]. There, we also test the restricted version of the NetWF that uses homogenized noise information, in line with the OS. Paired t -tests show that the full NetWF reduces MSE significantly relative to both the raw snapshots ($p = 0.01$) and the OS ($p = 0.03$), while the second-best restricted NetWF is still significantly better than the raw snapshots ($p = 0.02$).

Upon further testing the NetWF, we also found an interesting directional asymmetry in this network. If we modify Eq. 5 by using source-node similarity in place of target-node similarity, i.e. defining $S_{\overrightarrow{AB}, \overrightarrow{CD}} \equiv s_{A,C}^{\text{source}} s_{B,D}^{\text{source}}$, the NetWF delivers even stronger denoising results with an average MSE of 0.07 ± 0.01 , as shown in SI Figure [placeholder]. This suggests that similarity in sending behaviors might carry more information about the edge weight correlations. This example illustrates that although our proposed edge-similarity measure is generically applicable, even better performance can be achieved if the similarity measure is tailored to the structure of the specific network dataset.

Last, we turn to our second goal with this dataset, that is, denoising when C_n is unknown. In this setting,

we use a naïve proxy of noise level for both the NetWF and the OS, using the variance across edge weights in the observed single calendar-month snapshot as the homogeneous noise variance. Even under this under-specified condition, the NetWF achieves significantly lower average MSE (0.14 ± 0.01) compared to both the raw snapshots and the OS baseline (0.18 ± 0.03) according to paired t -tests, with p -values 0.02 and 0.04 respectively. Therefore, successful denoising is possible with the NetWF even with minimal inputs, as long as a reasonable noise level is assumed; see SI Figure [placeholder].

DISCUSSION

The Wiener filter was the first example of a statistically solid noise reduction technique [53]. The generalized Wiener filtering framework is mathematically grounded, as the Wiener operator (Eq. 2) optimally solves the MSE minimization problem (Eq. 1). Yet, an extension to even static network data remained an unsolved problem until now. Our proposed NetWF offers a qualitative advancement in addressing the often-overlooked issue of noise in static networks. It is a versatile denoising scheme that is applicable to both directed and undirected networks, with any weights, including signed networks. A key to this advancement is our proposed concept of edge-similarity, a generic solution that is intuitive and interpretable, building upon any preferred notion of node similarity.

An exciting future direction is to utilize the NetWF to identify the most suitable measure of node (or edge) similarity adaptively in each dataset that optimizes the output of the NetWF. As illustrated on the Enron email dataset, such notions of similarity that are tailored to

each application are expected to lead to further improved results. Another promising avenue is to use dimension reduction and machine learning techniques to learn the optimal similarity structure, such as using node2vec to generate low-dimensional node embeddings, which can then be used to model node and edge-similarities [54]. The NetWF naturally adapts to different levels of uncertainty in network data, see SI Figure [placeholder]. Although the NetWF is expected to perform best when a full noise characterization is available, we illustrated that in practice it is able to yield similarly good results even with much less information, such as a homogeneous noise estimate.

As large-scale biological data are inherently imperfect, this is a key area of application for the NetWF. As an illustration, we used a biologically coherent portion of the entire SGA GI dataset in the baker's yeast, where the strong reported structure of the data offered multiple reliable evaluations by comparing to benchmark datasets. A natural next step is to apply the NetWF to the entire yeast data as well as to similar data in other organisms, like the recent genome-scale screen in human HAP1 cells [55]. By reducing data noise, these applications could further clarify the amount of agreement between the functional architecture of various organisms.

As illustrated on the Enron dataset, the static NetWF is also applicable to snapshots over temporal networks. An opportunity for future development is a temporal NetWF that considers the full time series of network data, combining temporal Wiener filtering ideas with the NetWF. Further extensions include multiplex and multilayer networks [56, 57], as well as hypergraphs and simplicial complexes [58, 59]. Such higher-order interactions play an important role in genetics, as evidenced by the prevalence of GIs between sets of three genes in yeast [60, 61], and are also increasingly studied in computational social science [62, 63].

Just as with any form of quantitative data analysis, understanding and reporting uncertainties in networks is crucial, as these uncertainties can be leveraged to improve the overall quality and reliability of network-based inference. We believe that the NetWF is an important starting point towards a paradigm change in network science where reporting and utilizing noise characteristics for any network data is a valuable and integral part of understanding the underlying complex networks.

MATERIALS AND METHODS

Implementation of the NetWF

We consider an observed network on v nodes, represented by a demeaned adjacency matrix $A \in \mathbb{R}^{v \times v}$ and its vectorization $a = \text{vec}(A) \in \mathbb{R}^k$ with $k = v^2$, together with a noise covariance matrix $C_n \in \mathbb{R}^{k \times k}$ characterizing noise in the edge weights. We first compute node-level profile similarity networks (PSNs), symmetric matrices

whose elements are similarities between node pairs, as in Eqs. 3–4 for directed networks or Eq. 6 for undirected networks. We present two NetWF implementations: a direct NetWF and an iterative NetWF.

In the direct implementation of the NetWF, we first construct a network-informed signal covariance $C_u \in \mathbb{R}^{k \times k}$ from the observed topology. C_u is directly calculated from the PSNs using the matrix Kronecker product, following the exact protocols in Eqs. 5 and 7. We then set the overall signal variability in C_u by giving it a prefactor equal to the data variance across entries in A , thereby completing the construction of C_u . The direct NetWF then avoids explicit matrix inverse in Eq. 2, $G^W = C_u(C_u + C_n)^{-1}$ for numerical stability. To obtain the signal estimate $\hat{u} = G^W a$, we break down this $\hat{u} = C_u x$ computation into two steps: (i) solve the linear subproblem $(C_u + C_n + \epsilon I)x = a$ for $x \in \mathbb{R}^k$, where ϵ is a small positive number to assure that the matrix is well-conditioned; (ii) compute $\hat{u} = C_u x$. Finally, we reshape \hat{u} to arrive at the denoised adjacency matrix $\hat{U} = \text{unvec}(\hat{u})$. Note that this direct implementation quickly becomes infeasible for large complex networks, as storing C_u and C_n requires $O(v^4)$ memory.

Hence, we develop an alternative, iterative implementation of the NetWF, which reduces the memory burden to $O(v^2)$, as long as C_n is diagonal (i.e. noise is treated as uncorrelated across edges). The key is to avoid explicitly forming C_u . Since $C_u + C_n$ is symmetric and positive semidefinite, we deploy the conjugate gradient (CG) algorithm to efficiently solve the linear subproblem $(C_u + C_n)x = a$ with guaranteed numerical convergence [64]. Note that CG does not require explicit formation of $C_u + C_n$, but only its action on vectors. Consequently, in both the CG subproblem and the subsequent $C_u x$ computation, we exploit the Kronecker-product structure of C_u via the identity $(M_1 \otimes M_2)x = \text{vec}(M_2 \text{unvec}(x) M_1^T)$, reducing the dimensionality of the problem from $\mathbb{R}^{k \times k}$ to $\mathbb{R}^{v \times v}$. This step resolves the memory bottleneck and allows the NetWF to scale to large empirical systems.

Pseudocode for both the direct NetWF and the CG-based iterative NetWF are provided in SI Text [placeholder].

Singular value shrinkage

As a baseline network denoising technique, we implement the optimal shrinker (OS) of singular values developed by Gavish and Donoho [37]. The OS adopts the spectral theory of random matrices [32] and works under the assumption that the rank of the signal adjacency matrix is much smaller than its dimension. Conceptually, the OS procedure yields a denoised network by preserving the dominant global network patterns and suppressing fluctuations that are more likely to be noise. For a v -by- v matrix observed in homogeneous white noise of variance σ^2 , the OS performs singular value decomposi-

tion and shrinks each singular value y_i to

$$y_i^* = \begin{cases} \sqrt{y_i^2 - 4v\sigma^2}, & y_i \geq 2\sqrt{v}\sigma, \\ 0, & y_i < 2\sqrt{v}\sigma, \end{cases} \quad (9)$$

and the denoised matrix is obtained. If we are given heterogeneous edge-level noise as an input, we calculate the mean of the noise variances and use it as the σ^2 input.

Data processing

The *S. cerevisiae* GI network, along with the noise variance matrix, was constructed from the SGA results reported in Ref. [11]. We focus on the densely connected essential GI network (ExE), in which essential genes are perturbed using temperature-sensitive alleles. Because each gene pair may be assayed in two orientations (query vs. array), we symmetrize the data by averaging both the reported GI scores and their associated noise variances, resulting in an undirected, weighted network on 427 essential-gene nodes.

Note that the raw ExE matrix, as well as the corresponding variances, contains missing entries; in cross validation, we likewise mask entries to create additional missing values. In the cross validation, we also manually put in missing entries. Before ingesting the data into the NetWF or the OS, we impute missing noise variances with the sum of the mean of observed variances and the variance of observed GI scores, and then impute missing GI scores with the mean of observed GI scores.

The PPI benchmark network was obtained from Biogrid [43], version 5.0.253 (compiled on Dec. 25, 2025), at <https://thebiogrid.org>. We filtered interaction types to retain only physical association and direct interaction. The protein co-complex membership bench-

mark network was derived from the protein complex standard provided by Ref. [11] based on Refs. [42, 44]. The Gene Ontology (GO) co-annotation network was constructed following the protocol in Ref. [11], with the GO functional annotation data downloaded from the Saccharomyces Genome Database (SGD) [45] at <https://www.yeastgenome.org>.

The Enron email corpus was obtained from <https://www.cs.cmu.edu/~enron/>, using the latest May 7, 2015 release. Both the NetWF and the OS baseline can introduce self-links and negative edge weights, even when the input network contains no self-links or negative edge weights. For visualization and evaluation in the Enron application, we therefore remove self-links and truncate negative weights to zero for all denoised outputs.

Data and code availability

For full reproducibility of the NetWF results in this study, we provide relevant processed data and code at https://github.com/markzhao98/NetWF_paper.

ACKNOWLEDGMENTS

The authors acknowledge funding through the ‘CAREER: Network-based inference of complex biological interactions’ PHY-2440223 Physics of Living Systems (POLS) NSF CAREER Award, sponsored by the NSF 22-586 Faculty Early Career Development Program. We thank Bingjie Hao, Ruiting Xie, Anastasiya Salova, Eli Daniel Ganz, Maryn Carlson, Noshir Contractor, Michael Costanzo, and Charles Boone for their helpful comments and discussion. T.Z. and I.A.K. acknowledge support from the NSF-Simons National Institute for Theory and Mathematics in Biology, jointly funded by the U.S. National Science Foundation (Award No. 2235451) and the Simons Foundation (Award No. MP-TMPS-00005320).

[1] B. Bollobás, *Modern graph theory* (Springer Science & Business Media, 1998).

[2] D. Lazer, A. Pentland, L. Adamic, S. Aral, A.-L. Barabási, D. Brewer, N. Christakis, N. Contractor, J. Fowler, M. Gutmann, *et al.*, Computational social science, *Science* **323**, 721 (2009).

[3] A.-L. Barabasi and Z. N. Oltvai, Network biology: understanding the cell’s functional organization, *Nature Reviews Genetics* **5**, 101 (2004).

[4] M. Barthélémy, Spatial networks, *Physics Reports* **499**, 1 (2011).

[5] J. F. Donges, Y. Zou, N. Marwan, and J. Kurths, Complex networks in climate dynamics: Comparing linear and nonlinear network construction methods, *The European Physical Journal Special Topics* **174**, 157 (2009).

[6] D. Acemoglu, A. Ozdaglar, and A. Tahbaz-Salehi, Systemic risk and stability in financial networks, *American Economic Review* **105**, 564 (2015).

[7] A.-L. Barabási, The network takeover, *Nature Physics* **8**, 14 (2012).

[8] P. V. Marsden, Network data and measurement, *Annual Review of Sociology* **16**, 435 (1990).

[9] N. J. Krogan, G. Cagney, H. Yu, G. Zhong, X. Guo, A. Ignatchenko, J. Li, S. Pu, N. Datta, A. P. Tikuvisis, *et al.*, Global landscape of protein complexes in the yeast *saccharomyces cerevisiae*, *Nature* **440**, 637 (2006).

[10] C. Von Mering, L. J. Jensen, B. Snel, S. D. Hooper, M. Krupp, M. Foglierini, N. Jouffre, M. A. Huynen, and P. Bork, String: known and predicted protein–protein associations, integrated and transferred across organisms, *Nucleic Acids Research* **33**, D433 (2005).

[11] M. Costanzo, B. VanderSluis, E. N. Koch, A. Baryshnikova, C. Pons, G. Tan, W. Wang, M. Usaj, J. Hanchar, S. D. Lee, *et al.*, A global genetic interaction network maps a wiring diagram of cellular function, *Science* **353**, aaf1420 (2016).

- [12] M. Newman, *Networks* (Oxford University Press, 2018).
- [13] D. Liben-Nowell and J. Kleinberg, The link prediction problem for social networks, in *Proceedings of the Twelfth International Conference on Information and Knowledge Management* (2003) pp. 556–559.
- [14] A. Clauset, C. Moore, and M. E. Newman, Hierarchical structure and the prediction of missing links in networks, *Nature* **453**, 98 (2008).
- [15] T. Zhou, L. Lü, and Y.-C. Zhang, Predicting missing links via local information, *The European Physical Journal B* **71**, 623 (2009).
- [16] W. Liu and L. Lü, Link prediction based on local random walk, *Europhysics Letters* **89**, 58007 (2010).
- [17] B. Barzel and A.-L. Barabási, Network link prediction by global silencing of indirect correlations, *Nature biotechnology* **31**, 720 (2013).
- [18] L. Lü, L. Pan, T. Zhou, Y.-C. Zhang, and H. E. Stanley, Toward link predictability of complex networks, *Proceedings of the National Academy of Sciences* **112**, 2325 (2015).
- [19] M. Zhang and Y. Chen, Link prediction based on graph neural networks, in *Proceedings of the 32nd International Conference on Neural Information Processing Systems* (2018) pp. 5171–5181.
- [20] I. A. Kovács, K. Luck, K. Spirohn, Y. Wang, C. Pollis, S. Schlabach, W. Bian, D.-K. Kim, N. Kishore, T. Hao, *et al.*, Network-based prediction of protein interactions, *Nature Communications* **10**, 1240 (2019).
- [21] X.-W. Wang, L. Madeddu, K. Spirohn, L. Martini, A. Fazzone, L. Beccetti, T. P. Wytock, I. A. Kovács, O. M. Balogh, B. Benczik, *et al.*, Assessment of community efforts to advance network-based prediction of protein–protein interactions, *Nature Communications* **14**, 1582 (2023).
- [22] S. Feizi, D. Marbach, M. Médard, and M. Kellis, Network deconvolution as a general method to distinguish direct dependencies in networks, *Nature Biotechnology* **31**, 726 (2013).
- [23] B. Wang, A. Pourshafeie, M. Zitnik, J. Zhu, C. D. Bustamante, S. Batzoglou, and J. Leskovec, Network enhancement as a general method to denoise weighted biological networks, *Nature Communications* **9**, 3108 (2018).
- [24] J. Yu, J. Leng, D. Sun, and L.-Y. Wu, Network refinement: denoising complex networks for better community detection, *Physica A: Statistical Mechanics and its Applications* **617**, 128681 (2023).
- [25] C. T. Butts, Network inference, error, and informant (in) accuracy: a bayesian approach, *social networks* **25**, 103 (2003).
- [26] R. Guimerà and M. Sales-Pardo, Missing and spurious interactions and the reconstruction of complex networks, *Proceedings of the National Academy of Sciences* **106**, 22073 (2009).
- [27] M. E. Newman, Network structure from rich but noisy data, *Nature Physics* **14**, 542 (2018).
- [28] M. E. Newman, Estimating network structure from unreliable measurements, *Physical Review E* **98**, 062321 (2018).
- [29] T. P. Peixoto, Reconstructing networks with unknown and heterogeneous errors, *Physical Review X* **8**, 041011 (2018).
- [30] L. Peel, T. P. Peixoto, and M. De Domenico, Statistical inference links data and theory in network science, *Nature Communications* **13**, 6794 (2022).
- [31] J.-F. Cai, E. J. Candès, and Z. Shen, A singular value thresholding algorithm for matrix completion, *SIAM Journal on optimization* **20**, 1956 (2010).
- [32] F. Benaych-Georges and R. R. Nadakuditi, The singular values and vectors of low rank perturbations of large rectangular random matrices, *Journal of Multivariate Analysis* **111**, 120 (2012).
- [33] A. A. Shabalin and A. B. Nobel, Reconstruction of a low-rank matrix in the presence of gaussian noise, *Journal of Multivariate Analysis* **118**, 67 (2013).
- [34] R. R. Nadakuditi, Optshrink: An algorithm for improved low-rank signal matrix denoising by optimal, data-driven singular value shrinkage, *IEEE Transactions on Information Theory* **60**, 3002 (2014).
- [35] M. Gavish and D. L. Donoho, The optimal hard threshold for singular values is $4/\sqrt{3}$, *IEEE Transactions on Information Theory* **60**, 5040 (2014).
- [36] J. Josse and S. Sardy, Adaptive shrinkage of singular values, *Statistics and Computing* **26**, 715 (2016).
- [37] M. Gavish and D. L. Donoho, Optimal shrinkage of singular values, *IEEE Transactions on Information Theory* **63**, 2137 (2017).
- [38] V. Thibeault, A. Allard, and P. Desrosiers, The low-rank hypothesis of complex systems, *Nature Physics* **20**, 294 (2024).
- [39] A. V. Oppenheim and G. C. Verghese, *Signals, systems & inference* (Pearson London, UK, 2017).
- [40] W. K. Pratt, Generalized wiener filtering computation techniques, *IEEE Transactions on Computers* **100**, 636 (2006).
- [41] Y.-Y. Ahn, J. P. Bagrow, and S. Lehmann, Link communities reveal multiscale complexity in networks, *Nature* **466**, 761 (2010).
- [42] A. Baryshnikova, M. Costanzo, Y. Kim, H. Ding, J. Koh, K. Toufighi, J.-Y. Youn, J. Ou, B.-J. San Luis, S. Bandyopadhyay, *et al.*, Quantitative analysis of fitness and genetic interactions in yeast on a genome scale, *Nature Methods* **7**, 1017 (2010).
- [43] R. Oughtred, J. Rust, C. Chang, B.-J. Breitkreutz, C. Stark, A. Willem, L. Boucher, G. Leung, N. Kolas, F. Zhang, *et al.*, The biogrid database: A comprehensive biomedical resource of curated protein, genetic, and chemical interactions, *Protein Science* **30**, 187 (2021).
- [44] J. J. Benschop, N. Brabers, D. van Leenen, L. V. Bakker, H. W. van Deutekom, N. L. van Berkum, E. Apweiler, P. Lijnzaad, F. C. Holstege, and P. Kemmeren, A consensus of core protein complex compositions for *Saccharomyces cerevisiae*, *Molecular cell* **38**, 916 (2010).
- [45] J. M. Cherry, E. L. Hong, C. Amundsen, R. Balakrishnan, G. Binkley, E. T. Chan, K. R. Christie, M. C. Costanzo, S. S. Dwight, S. R. Engel, *et al.*, *Saccharomyces* genome database: the genomics resource of budding yeast, *Nucleic Acids Research* **40**, D700 (2012).
- [46] J. Van Leeuwen, C. Pons, J. C. Mellor, T. N. Yamaguchi, H. Friesen, J. Koschwanez, M. M. Ušaj, M. Pechlaner, M. Takar, M. Ušaj, *et al.*, Exploring genetic suppression interactions on a global scale, *Science* **354**, aag0839 (2016).
- [47] J. Van Leeuwen, C. Pons, G. Tan, J. Z. Wang, J. Hou, J. Weile, M. Gebbia, W. Liang, E. Shuteriqi, Z. Li, *et al.*, Systematic analysis of bypass suppression of essential genes, *Molecular Systems Biology* **16**, MSB209828 (2020).

- [48] K. Mei and W. Guo, The exocyst complex, *Current Biology* **28**, R922 (2018).
- [49] A.-C. Gavin, P. Aloy, P. Grandi, R. Krause, M. Boesche, M. Marzioch, C. Rau, L. J. Jensen, S. Bastuck, B. Dümpelfeld, *et al.*, Proteome survey reveals modularity of the yeast cell machinery, *Nature* **440**, 631 (2006).
- [50] J. A. Songer and M. Munson, Sec6p anchors the assembled exocyst complex at sites of secretion, *Molecular Biology of the Cell* **20**, 973 (2009).
- [51] B. Klimt and Y. Yang, The enron corpus: A new dataset for email classification research, in *Machine Learning: ECML 2004* (2004) pp. 217–226.
- [52] P. Csermely, A. London, L.-Y. Wu, and B. Uzzi, Structure and dynamics of core/periphery networks, *Journal of Complex Networks* **1**, 93 (2013).
- [53] N. Wiener, *Extrapolation, interpolation, and smoothing of stationary time series: with engineering applications* (MIT Press, 1949).
- [54] A. Grover and J. Leskovec, node2vec: Scalable feature learning for networks, in *Proceedings of the 22nd ACM SIGKDD international conference on Knowledge discovery and data mining* (2016) pp. 855–864.
- [55] M. Billmann, M. Costanzo, X. Zhang, A. Z. Hassan, M. Rahman, K. R. Brown, K. S. Chan, A. H. Y. Tong, C. Pons, H. N. Ward, *et al.*, A global genetic interaction map of a human cell reveals conserved principles of genetic networks, *bioRxiv* (2025).
- [56] S. Boccaletti, G. Bianconi, R. Criado, C. I. Del Genio, J. Gómez-Gardenes, M. Romance, I. Sendina-Nadal, Z. Wang, and M. Zanin, The structure and dynamics of multilayer networks, *Physics Reports* **544**, 1 (2014).
- [57] M. Kivelä, A. Arenas, M. Barthelemy, J. P. Gleeson, Y. Moreno, and M. A. Porter, Multilayer networks, *Journal of Complex Networks* **2**, 203 (2014).
- [58] F. Battiston, G. Cencetti, I. Iacopini, V. Latora, M. Lucas, A. Patania, J.-G. Young, and G. Petri, Networks beyond pairwise interactions: Structure and dynamics, *Physics Reports* **874**, 1 (2020).
- [59] G. Bianconi, *Higher-order networks* (Cambridge University Press, 2021).
- [60] E. Kuzmin, B. VanderSluis, W. Wang, G. Tan, R. Deshpande, Y. Chen, M. Usaj, A. Balint, M. Mattiazzi Usaj, J. Van Leeuwen, *et al.*, Systematic analysis of complex genetic interactions, *Science* **360**, eaao1729 (2018).
- [61] E. Kuzmin, M. Rahman, B. VanderSluis, M. Costanzo, C. L. Myers, B. J. Andrews, and C. Boone, τ -sga: Synthetic genetic array analysis for systematically screening and quantifying trigenic interactions in yeast, *Nature Protocols* **16**, 1219 (2021).
- [62] F. Shi, J. G. Foster, and J. A. Evans, Weaving the fabric of science: Dynamic network models of science’s unfolding structure, *Social Networks* **43**, 73 (2015).
- [63] A. Lungeanu, D. R. Carter, L. A. DeChurch, and N. S. Contractor, How team interlock ecosystems shape the assembly of scientific teams: A hypergraph approach, in *Computational Methods for Communication Science* (Routledge, 2021) pp. 95–119.
- [64] G. H. Golub and C. F. Van Loan, *Matrix computations* (Johns Hopkins University Press, 2013).